On the two classes of global primary modal instability in laminar separation bubbles

Daniel Rodríguez[1,2]*, Elmer M. Gennaro[1]†, and Matthew P. Juniper[3]‡

[1]*Escola de Engenharia de São Carlos, Universidade de São Paulo, Brazil*

[2]*School of Aeronautics, Universidad Politécnica de Madrid, Spain*

[3]*Department of Engineering, University of Cambridge, CB2 1PZ, UK.*

The self-excited global instability mechanisms existing in flat-plate laminar separation bubbles are studied here, in order to shed light on the causes of unsteadiness and three-dimensionality of unforced, nominally two-dimensional separated flows. The presence of two known linear global mechanisms, namely an oscillator behavior driven by local regions of absolute inflectional instability and a centrifugal instability giving rise to a steady three-dimensionalization of the bubble, is studied in a series of model separation bubbles. Present results indicate that absolute instability, and consequently a global oscillator behavior, does not exist for two-dimensional bubbles with a peak reversed-flow velocity below 12% of the free-stream velocity. However, the three-dimensional instability becomes active for recirculation levels as low as $u_{\mathrm{rev}} \approx 7\%$. These findings suggest a route to the three-dimensionality and unsteadiness observed in experiments and simulations substantially different from that usually found in the literature, in which two-dimensional vortex shedding is followed by three-dimensionalization.

I. Introduction

Flow separation is invariably associated with adverse effects on the performance of lifting surfaces, a reason which has provided motivation for research efforts spanning over more than half a century. However, and despite the continuous research, many questions related to the appearance, structure and behavior of separation bubbles remain open. Some of these questions were first referred to in the works of Gault and McCullough[1–3] regarding the aerodynamic characteristics of airfoils near and at post stall conditions. They noted the existence of three different kinds of laminar separation bubbles: for relatively thick airfoils, separation takes place near the trailing edge and moves up-chord with increasing angle of attack; the involved physics are similar to those on bluff-bodies. On the other hand, for thin airfoils separation occurs near the leading edge, immediately past the suction peak. Leading edge bubbles are then divided into *short* and *long* according to their extent in the streamwise direction, and have a very different impact on the aerodynamic properties of the airfoil. The process in which a short bubble suddenly fails to reattach and becomes a long bubble after a small variation on angle of attack or Reynolds number is referred to as *bursting*;[4] its physical causes and the determination of an adequate criteria for predicting its occurrence have been since the 60's, and are still today, an active topic of research.[4–8]

The usual picture of inviscid instability of the separated shear layer leading to laminar-turbulent transition, and turbulent mixing being ultimately responsible for the reattachment of the separation bubble suggested considering the properties of the boundary-layer at separation as a criterion for bursting. Besides bursting, the prediction of other characteristics of separated flow like the onset of unsteadiness (sometimes associated directly with bursting[6]) or three-dimensionalization of nominally two-dimensional laminar separation bubbles[9,10] has been attempted through the study of linear instability mechanisms of the flow. The

*Marie Curie COFUND fellow, Escola de Engenharia de São Carlos, Universidade de São Paulo, Brazil and Universidad Politécnica de Madrid, Spain. AIAA Member. dani@torroja.dmt.upm.es

†Postdoctoral Scholar, Escola de Engenheria de São Carlos, Universidade de São Paulo, Brazil.

‡Professor, Department of engineering, University of Manchester, UK.

presence and dominance of Kelvin-Helmholtz instability acting on the shear layer has been confirmed in a multitude of experimental[11,12] and numerical investigations.[6,8,9,13,14] However, Kelvin-Helmholtz (K-H) instability alone does not suffice to explain either the occurrence or breathing or flapping bubble behavior, i.e. oscillations of the entire separation bubble at frequencies substantially lower than those predicted by locally-parallel linear stability theory.

Theoretical interest in global instability of separation bubbles, either viewed as the existence of an oscillator behavior driven by spatial regions of absolute instability in weakly non-parallel flow[15,16] or as the linear instability of a fully non-parallel base state,[17,18] has gained momentum in recent years.

The instability properties of wave-like disturbances like the K-H instability mechanism have been addressed in the past by means of analyses based on the locally-parallel flow approximation. External instability waves arriving at the separated region experience a growth of several orders-of-magnitude caused by the inflectional instability of the shear layer, eventually leading to nonlinear effects and vortex shedding unless the initial amplitudes were very small. This description of laminar separation bubbles as amplifiers of external perturbations does not, however, suffice to explain the onset of unsteadiness observed in direct numerical simulations (DNS) of unperturbed separated flow, nor the occurrence or breathing or flapping bubble behavior. Absolute/convective instability analysis[19] suggested that, besides the amplifier character of the bubbles, they can also act as oscillators when a spatial region of the underlying base state can sustain instability waves that propagate upstream. A global instability mechanism would exist in this case, intrinsic to the bubble, that ultimately results in vortex shedding. Some theoretical studies were conducted in the past studying this possibility.[20,21]

On the other hand, global instability analysis without resorting to locally-parallel flow approximations has experienced increased activity in the last decade following the advances in computational capabilities necessary to support the associated numerical work.[18] Following this approach, the stability of the two-dimensional base state under perturbations with arbitrary shape is studied by means of partial-derivative-based eigenvalue problems. Consequently, the analysis is not restricted to wave-like disturbances, but any three-dimensional modal perturbation is considered, enabling the study of instability mechanisms different from the K-H instability. Worthy of mention is the work of Dallmann and Schewe,[22] in which they postulate the existence of a global instability mechanism acting on nominally two-dimensional separation bubbles, which would exert a three-dimensionalization of the flow eventually leading to unsteadiness. They regret the absence, at that time, of an analysis methodology able to address this kind of instability. It was not until the work of Theofilis *et al.*[23] that the required global (or BiGlobal) stability analysis was applied to a separation bubble on a flat-plate, demonstrating the existence of a self-excited three-dimensional instability mode and proposing an origin for the unsteadiness of separation bubbles alternative to inflectional instability. Similar results have been reported in other geometries comprising two-dimensional recirculation regions.[24–27] Studies of the topological changes exerted by the three-dimensional instability both on flat-plate laminar separation bubbles[28] (representative of leading-edge bubbles) and in a stalled NACA 0015 airfoil[29] (i.e. a trailing-edge bubble) related the mentioned three-dimensional global instability mode to separation cellular patterns or stall cells that have been observed experimentally at high Reynolds numbers.[30–32]

A question that remains open is the ability to predict the onset of global instability in separated flow on the basis of base or mean flow measurements and a simple criterion. In this respect, Huerre and Monkewitz[19] proposed that the criterion $u_{\text{rev}} = u^*_{\text{rev}}/U^*_\infty > 15\%$ relating the peak value of the reversed flow to the free-stream velocity, be used to define the onset of absolute instability in the shear layer profile. This value is in contrast with absolute/convective analyses of shear layers in the presence of a wall[20,21,33] (a geometry more related to laminar separation bubbles), that agree in a value around $u_{\text{rev}} \approx 20 - 30\%$ for the onset of absolute instability, in line with results from DNS.[34] Conversely, unsteadiness and vortex shedding have been reported consistently in three-dimensional simulations in which the peak reversed flow of the mean flow is $u_{\text{rev}} \approx 10\%$, remarkably lower than the $20 - 30\%$ necessary for absolute instability of linear disturbance waves.[9,35,36] Scenarios of global instability have been postulated[22,23,37] in order to explain the origin of unsteadiness, but the identification of such global instability mechanisms and the associated criteria is still lacking. Building upon previous ideas,[23,28] the possibility of a route to unsteadiness different from the self-sustained two-dimensional K-H instability was investigated recently.[38] A series of flat-plate laminar separation bubble models were constructed and two instability mechanisms were analyzed, namely the amplification of external perturbations by K-H instability and the three-dimensional global instability. It was concluded that the model bubbles were too weak, in terms of peak reversed flow, for the K-H to be absolutely unstable, while the three-dimensional global mode was found to become unstable for peak reversed

flows as low as $u_{\rm rev} = 7\%$: the primary bifurcation from the steady two-dimensional base state in those cases is a three-dimensionalization, which could serve as the triggering mechanism leading to three-dimensional unsteady states. However, the set of bubble models considered in that work was very limited, and proper instability analyses aimed to the study of the global oscillator mechanism was not performed.

This work revisits the global instability of nominally two-dimensional laminar separation bubbles on a flat-plate, with three main novelties with respect to the aforementioned work.[38] First, the set of base separation bubbles has been enlarged in order to ascertain if the conclusions drawn correspond to a very particular choice of parameters or if they can be considered as representative of more general cases. The second novelty is the search for global instability mechanisms based on local regions of absolute instability of disturbance waves, following an approach similar to that of Hammond and Redekopp.[21] The third subject of study, no less important, is an effort in the unification of the results of the two approaches of global instability analysis used herein. In a recent work, Juniper *et al.*[39] compared the growth rates, frequencies and perturbation shapes of the leading global mode computed by the two types of analysis for a confined planar wakes showing good agreement in that configuration.

The rest of the paper is organized as follows. Section II describes an inverse formulation of the boundary-layer equations which is subsequently used in order to construct a set of model laminar separation bubbles on a flat-plate. The two approaches to the study of linear instability considered in the paper are outlined in section III. Section IV.A presents results of the locally-parallel flow analysis, while results for the three-dimensional global instability mode, obtained using the partial-derivative-based global instability analysis are presented in section IV.B. A brief exposition of the results and conclusions close the paper.

II. Base flow construction

A. Inverse formulation of the non-similar boundary-layer problem

A non-similar inverse formulation of the boundary-layer equations on a flat plate is used to obtain the base flow. In choosing the current non-similar boundary-layer formulation, the possibility of the appearance of the bubble shedding as the peak reversed flow increases is circumvented in the computation of the base flow and may be subsequently recovered as a global instability of the flow.

The physical dimensional streamwise x^* and wall-normal y^* coordinates, an arbitrary characteristic length in the streamwise direction L^*, the far-field velocity U_e^*, and the kinematic viscosity ν^* are used to define the non-dimensional boundary-layer variables

$$\xi = x^*/L^*, \quad \text{and } \eta = y^*\sqrt{U_e^*/\ \nu^* x^*}, \tag{1}$$

and a transformed stream-function

$$f(\xi,\eta) = \Psi/\sqrt{U_e^*\nu^* x^*}. \tag{2}$$

Introducing these variables into the streamwise momentum equation, an equation for the transformed stream-function $f(\xi,\eta)$ is obtained. In order to recover separated states, the (FLARE) Reyhner and Flügge-Lotz approximation[40] has been invoked, which neglects the streamwise convective term when reversed flow exists. The boundary-layer equation is written as

$$f_{\eta\eta\eta} + \frac{m+1}{2} f f_{\eta\eta} + m(1 - f_\eta^2) = \xi(\theta f_\eta f_{\xi\eta} + f_{\eta\eta} f_\xi), \tag{3}$$

where subscripts denote partial differentiation, and $m = \frac{\xi}{U_e^*}\frac{dU_e^*}{d\xi}$ is the deceleration parameter, which is variable with ξ. The FLARE approximation appears in this equation as the function θ, which takes value unity when $f_\eta \geq 0$ and vanishes if $f_\eta < 0$. This problem is solved subjected to the boundary conditions

$$f(\xi,0) = 0, \quad f_\eta(\xi,0) = 0, \quad \text{and} \quad f_\eta(\xi,\eta\to\infty) \to 1. \tag{4}$$

In order to avoid Goldstein's singularity, which would appear at the separation point if a $m(\xi)$ distribution were imposed, the displacement thickness measured in the transformed variable η is imposed here as an asymptotic boundary condition:

$$f(\xi,\eta\to\infty) \to 1 - \bar{\delta}(\xi). \tag{5}$$

The solution algorithm iterates on each ξ profile until a converged profile $f(\xi,\eta)$ and $m(\xi)$ are obtained. The complete derivation of the equation and boundary conditions can be found in Cebeci and Cousteix;[40] further details on the solution procedure were presented in Rodríguez and Theofilis.[28]

B. The boundary-layer-based LSB model base flows

The two-dimensional LSB base state $\bar{\mathbf{q}}$ is constructed using the calculated transformed stream-function $f(\xi,\eta)$ (2). The streamwise and wall-normal dimensional velocity components are obtained using the transformation (1,2):

$$u^* = U_e^* \cdot f_\eta, \tag{6}$$

$$v^* = \frac{1}{2}\sqrt{\frac{U_e^*\nu}{\xi}}\left[f(m+1) + 2\xi f_\xi + \eta f_\eta(m-1)\right]. \tag{7}$$

Lengths are scaled using the dimensional displacement thickness at the inflow boundary, δ^*_{in}, while the physical streamwise and wall-normal velocity components u^* and v^*, and their first derivatives are made dimensionless using the inflow far-field velocity, U^*_∞, and δ^*_{in}. The non-dimensional spatial variables are denoted by x and y and the base flow dimensionless velocities by $\bar{u}$ and $\bar{v}$. The reference displacement thickness δ^*_{in} chosen corresponds to $Re_{\text{in}} = 450$. The respective inflow coordinate is $x = 152$.

An analytical distribution of displacement thickness analogous to that prescribed by Carter[41] is used for (5), in which $\bar{\delta}$ starts at the Blasius value (1.7208) at the inflow boundary, is increased within a finite extent until a maximum thickness $\bar{\delta}_{\max}$ is attained; then is decreased until the Blasius solution is again recovered and is kept constant until the outflow boundary:

$$\bar{\delta}(x) = (\bar{\delta}_{\max} - \bar{\delta}_B)\cdot[S(\xi_1) - S(\xi_2)] + \bar{\delta}_B, \tag{8}$$

where

$$S(\xi) = \begin{cases} 0, & \xi < 0 \\ \left[1 + \exp\left(\frac{1}{\xi-1} + \frac{1}{\xi}\right)\right]^{-1}, & 0 \le \xi \le 1 \\ 1, & 1 < \xi \end{cases} \tag{9}$$

and the auxiliary non-dimensional coordinates ξ_1 and ξ_2 are defined as

$$\xi_1 = a\frac{2(x-x_1)}{x_2-x_1}, \quad \xi_2 = a\frac{2x-x_1-x_2}{x_2-x_1}. \tag{10}$$

The coordinates x_1 and x_2 define the locations where the increase of displacement thickness starts and ends. While delivering displacement thickness distributions analogous to the piece-wise polynomial distributions used in other works,[41,42] the present function has the advantage of continuous derivatives of all orders. The value $\bar{\delta}_{\max}$ acts as a parameter defining the strength of the laminar separation bubble in terms of both bubble height and reversed flow. $\bar{\delta}_B = 1.72078$ is the displacement thickness corresponding to the Blasius velocity profile. The parameter a is used to determine the maximum slope of S, and was fixed at $a = 0.65$. As a result of the choice of the parameter a, the actual maximum displacement thickness of the bubble is $\delta_{\max} \approx 0.96 \times \bar{\delta}_{\max}$, and the effective locations of the start and end of the increase of displacement thickness are slightly displaced from of x_1 and x_2.

A series of base flows are computed varying the parameters x_2 and $\bar{\delta}_{\max}$. The coordinate $x_1 = 210$ is kept fixed and three different streamwise extents were considered: $x_2 = 264$, 290 and 320. For each extent, the value $\bar{\delta}_{\max}$ is varied from 3 to 10. In what follows the different base flows are designated by a letter and a number: the letter corresponds to the deceleration extent, S for short, M for medium and L for long bubbles; the number corresponds to the $\bar{\delta}_{\max}$ value. Figures 1 and 2 summarizes the characteristic parameters of the model separation bubbles. Figure 1 shows the location of the separation and reattachment points for each model bubble, as well as the location of the negative peak of wall shear $\tau = f_{\eta\eta}$. In the cases where $\bar{\delta}_{\max}$ is low, the wall shear distribution within the separated region is nearly symmetric, and consequently the recirculation center within the bubble is close to the center of the deceleration region. As $\bar{\delta}_{\max}$ is increased the peak wall-shear is increased and displaced downstream, and therefore the recirculation center moves

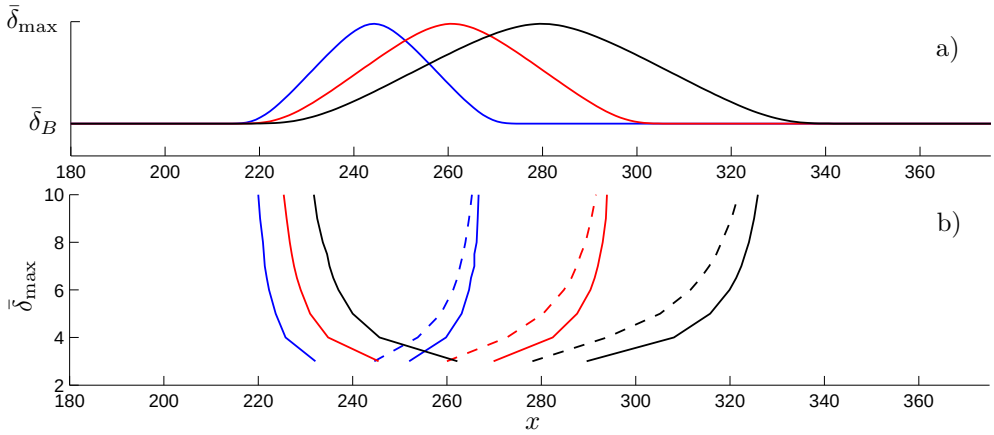

Figure 1. Laminar separation bubble models. a) transformed displacement thickness distribution $\bar{\delta}$. b) Extent of the reversed flow region as a function of $\bar{\delta}_{\max}$. Solid lines denote separation and reattachment line and dashed line denote the location of the peak negative wall-shear $\tau_{\min}$. Blue, red and black lines correspond to cases S, M and L, respectively.

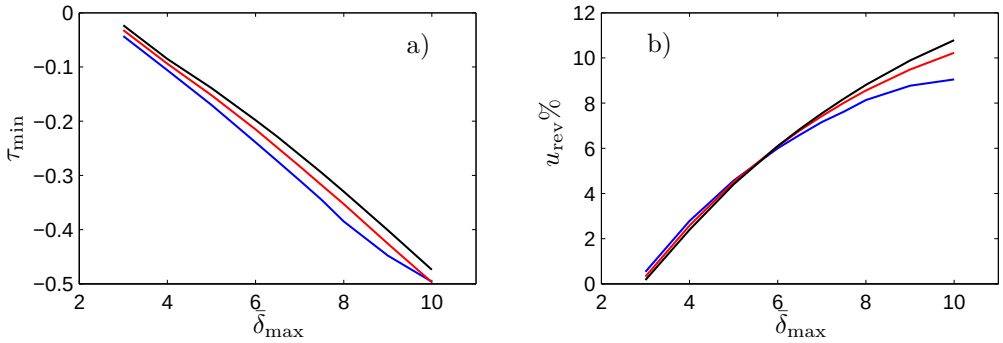

Figure 2. Peak negative wall shear $\tau_{\min}$ (a) and reversed flow $u_{\text{rev}}\%$ (b) as a function of $\bar{\delta}_{\max}$. Blue, red and black lines correspond to cases S, M and L, respectively.

downstream resulting into an asymmetric bubble. Figure 2 shows the peak values of the negative wall shear and the reversed flow, scaled with the inflow free-stream velocity $u_{\text{rev}} = u^*_{\text{rev}}/U^*_\infty$.

III. Linear stability analysis methodologies

Linear stability analysis studies the evolution of perturbations of infinitesimal amplitude superimposed upon a steady solution of the Navier-Stokes equations, referred to as the base flow. The base flows $\bar{\mathbf{q}} = (\bar{u}, \bar{v})$ considered here have an inhomogeneous dependence on the streamwise x and wall-normal y coordinates.

Two different types of linear instability analysis are used in this work. The first method considers two-dimensional wave-like perturbations with a downstream evolution determined by the local properties of the base flow. The WKBJ approximation is employed, assuming that the characteristic length for the streamwise variations of the base flow is much larger than the wavelengths λ_x of the dominant instability waves. This separation in scales permits reducing the analysis to the solution of several one-dimensional generalized matrix eigenvalue problems (EVP) at each axial location X, or slice. The absolute frequency ω_0 is computed at each slice, and the complex frequency of the global mode ω_g is estimated by analytical continuation into the complex X-plane. The response of each slice at ω_g is then computed and the WKBJ approximation is inverted in order to obtain the modal shape $\hat{\mathbf{q}}(X, y)$. This type of analysis is described further in section III.A.

The second method does not impose any assumption on the shape of the perturbations. Following from the dimensionality of the base flow and using separation of variables, modal linear perturbations can be written, without loss of generality, as $\hat{\mathbf{q}}(x, y)\exp[\mathrm{i}(\beta z - \omega t)]$. Introducing this decomposition into the linearized Navier-Stokes equations (LNSE), one arrives at a partial-derivative-based eigenvalue problem for

two-dimensional eigenfunctions, as discussed in section III.B.

A. The local instability analysis

The local analysis assume that the flow exhibits two well-separated length scales: an instability wavelength, λ_x, and a length scale that characterizes the stream-wise non-uniformity of the base flow, L. The ratio $\epsilon = \lambda_x/L$ must be small for a local analysis to be rigorously valid. The current development follows Monkewitz *et al.*,[15] which is summarized pedagogically in Huerre and Monkewitz.[43] The linearized Navier-Stokes equations (LNSE) contain terms that scale with ϵ^0, terms that scale with ϵ^1 and terms, which are neglected, that scale with higher powers of ϵ.

The $O(\epsilon^0)$ terms represent a streamwise succession of locally parallel eigenvalue problems (EVPs) for the local instability at each slice X. The LNSE are expressed as three partial differential equations (PDEs) in three primitive variables, $\hat{\mathbf{q}} = (\hat{u}, \hat{v}, \hat{p})^T$, and Fourier modes are introduced along the streamwise direction, leading to

$$\mathbf{q}'(x, y, t) = \hat{\mathbf{q}}(y) \exp[\mathrm{i}(kx - \omega t)]. \tag{11}$$

This converts the three PDEs into three ordinary differential equations (ODEs), that are discretized on a Chebyshev-spaced grid in the y-direction producing a generalized matrix EVP of the form

$$\mathbf{A}(k)\phi = \omega \mathbf{B}(k)\phi \tag{12}$$

where ϕ is a column vector representing the discretized values of $\hat{\mathbf{q}}$. This is satisfied for certain (ω, k) pairs and represents the dispersion relation for this slice of the flow. A spatio-temporal stability analysis is performed by finding the saddle points of $\omega(k)$ that are also k^+/k^- pinch points. These saddle points are then followed as the base flow evolves downstream. The absolute complex frequency of the dominant saddle, ω_0, as a function of streamwise distance, X, is stored for the next step in the analysis.

The complex frequency of the linear global mode, ω_g, is given at leading order in ϵ by the saddle point of $\omega_0(X)$, which is labeled $\omega_s(X_s)$.[44] For this, it is assumed that the absolute complex frequency $\omega_0(X)$ can be continued analytically into the complex X-plane. The position of the saddle point X_s is estimated by selecting the region of $\omega_0(X)$ around the maximum of $\omega_{0i}(X)$ and then fitting Padé polynomials to these values. Padé polynomials have two advantages over standard polynomials: they can fit $\omega_0(X)$ accurately at relatively low order, and they are better behaved in the complex plane.[45]

The two-dimensional global mode shape is finally calculated by investigating how the flow responds to an oscillation with complex frequency ω_g, by evaluating the integral

$$\mathbf{q}'(x, y, t) \sim A_0(X)\hat{\mathbf{q}}^{\pm}(y; X) \exp\left(\frac{\mathrm{i}}{\epsilon}\int_0^X k^{\pm}(X'; \omega)\, dX' - \omega_g t\right) + c.c., \tag{13}$$

where the results of the corresponding local EVPs are used at the X-position of each slice: k^+ and k^- are respectively the local wavenumbers downstream and upstream of the wavemaker X_s, computed as the values k that satisfy (12) when $\omega = \omega_g$. Similarly, $\hat{\mathbf{q}}^{\pm}(y; X)$ is the corresponding local eigenfunction downstream and upstream of X_s. The global mode is estimated by integrating the k^- branch upstream of X_s and the k^+ branch downstream of X_s. The $O(\epsilon^1)$ terms of the LNSE describe the evolution of the slowly-varying amplitude $A_0(X)$. In this paper, we assume that A_0 is uniform. In Juniper *et al.*,[39] it was concluded that the influence of this assumption is much smaller than the influence of the inaccuracies in $k^{\pm}$. More details on this analysis method can be found in that reference.

B. The global instability analysis

The global (or BiGlobal) instability analysis considers any functional shape for the perturbations that is allowed by the description of the base flow. The present base flow being inhomogeneous in the streamwise and wall-normal directions x and y, the most general modal perturbations can be expressed as

$$\mathbf{q}'(x, y, z, t) = \hat{\mathbf{q}}(x, y) \exp[\mathrm{i}(\beta z - \omega t)] + c.c. \tag{14}$$

where β is a wavenumber in the spanwise direction, corresponding to a periodicity length $\lambda_z = 2\pi/\beta$. Substitution of (14) into the LNSE delivers a PDE-based eigenvalue problem that, after discretization, takes the form

$$\mathbf{A}(\beta)\phi = \omega\mathbf{B}\phi. \tag{15}$$

Here the vector ϕ contains the discretized version of the eigenfunctions $\hat{\mathbf{q}}(x, y)$, associated with the global complex frequency ω. Stability analysis based on the solution of PDE-based EVPs is often limited by the large size of the matrices $\mathbf{A}$ and $\mathbf{B}$ resulting from the numerical discretization of the linear operators involved. Iterative algorithms based on Krylov subspace iteration have been shown to be very efficient when a reduced window of the eigenspectrum, localized around a pre-defined value σ, is sought for. In particular, the shift-and-invert Arnoldi algorithm has become widely popular in the solution of this kind of EVPs.[17,18]

In our previous works[28,39,46] we used different implementations of a similar algorithm for the solution of the EVP, using a spectral collocation discretization and the parallel dense linear algebra library ScaLAPACK. In this manner, the memory limitations can be by-passed by using distributed-memory machines, but a large amount of computational resources is still required. In this work, we make use of a novel algorithm[47] that combines a 8th-order finite differences discretization with sparse storage and operation of the matrices. The most demanding task in the Arnoldi algorithm, namely the formation and LU decomposition of the matrix $\mathbf{A} - \sigma\mathbf{B}$, is performed using the open-source library MUMPS.[48] The computational resources required for the solution of one EVP of the class (15) in Rodríguez and Theofilis[28] were 460 Gb. and nearly 4 hours of wall-clock time in JUGENE (www.fz-juelich.de/jsc/jugene); using the present algorithm, the solution of the same EVP to a similar convergence level can be obtained in a desktop computer in few minutes, thus enabling the parametric study presented in this work. The new algorithm also permits the use of spatial resolutions higher than those affordable with the previous approach. The maximum spatial resolution considered in the present work makes use of $N_x \times N_y = 1800 \times 400$ points, requiring approximately of 50 Gb. and 3 hours for the recovery of the leading 1000 eigenmodes on a shared memory machine featuring two intel Xeon E5-2690 processors.

IV. Results of the linear instability analyses

The presence of two linear global instabilities in the model laminar separation bubbles is studied here: a two-dimensional global oscillator resulting from the existence of regions of absolute instability of the K-H waves, and the steady three-dimensional global mode of laminar separation bubbles discovered by Theofilis *et al.*[23]

A. Two-dimensional global oscillator

Laminar separation bubbles are known to act as amplifiers of incoming disturbance waves, giving rise to amplifications orders of magnitude larger than those associated with zero-pressure-gradient or attached adverse-pressure-gradient boundary layers at the same Reynolds numbers. However, as far as this local instability is of convective nature, it does not suffice to explain the onset of self-sustained oscillations on the bubble. In the case that the local instability analysis predicts an absolute instability of the waves, a global mechanism can exist leading to synchronized oscillations in the absence of external excitation. This possibility was suggested in the past[6,20,21] to be responsible for the unsteadiness in separation bubbles, but a large peak reversed flow $u_{\text{rev}} \geq 20\%$ was found to be required for the existence of the unstable oscillator mode. Here, the local instability analysis described in section III.A is employed in order to determine whether the present family of model bubbles, with $u_{\text{rev}} < 12\%$ can behave as global oscillators.

Figure 3 shows the maximum absolute growth rate $\omega_{0,i}$ and the streamwise location where it is attained. The least stable region corresponds in all cases to the vicinity of the maximum displacement thickness of the bubble, where the inflection point is farther from the wall, as expected from other local stability analysis of shear flows.[19,33] The peak reversed flow occurs downstream of the peak displacement thickness and consequently it is not the most representative quantity for the local analyses. No regions of absolute instability were found for any of the model bubbles. In any case, figure (3,(a)) suggests that a base flow with a peak reversed flow much larger than 12% would be required for the onset of absolute instability.

Figure 4 shows the frequency and growth rate corresponding to the global oscillator mode. Without local regions of absolute instability, the oscillator mode is stable for all the model bubbles analyzed. The global

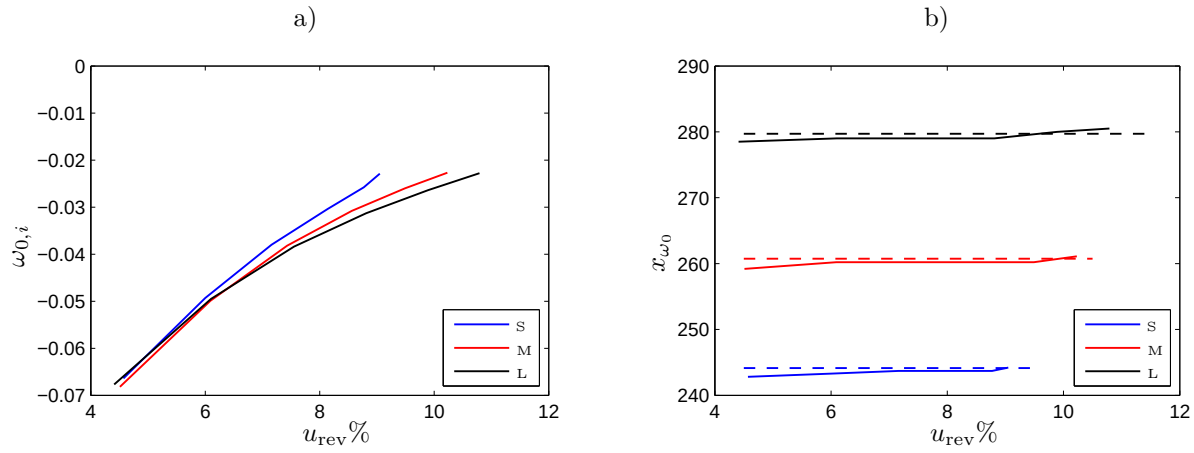

Figure 3. Maximum absolute growth rate $\omega_{0,i}$ (a) and corresponding streamwise coordinate (b) as a function of the peak reversed flow $u_{\mathrm{rev}}\%$. The dashed lines denote the location of the peak displacement thickness, $\bar{\delta}_{\max}$. Blue, red and black lines correspond to cases S, M and L, respectively.

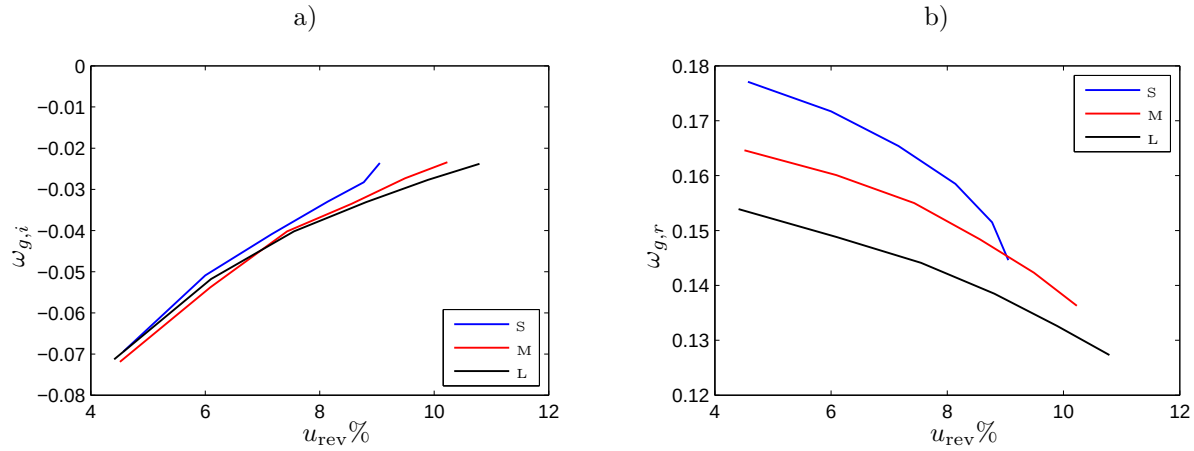

Figure 4. Growth rate (a) and frequency (b) corresponding to the global oscillator mode as a function of the peak reversed flow $u_{\mathrm{rev}}\%$. Blue, red and black lines correspond to cases S, M and L, respectively.

growth rate $\omega_{g,i}$ follows closely the maximum absolute growth rate $\omega_{0,i}$, highlighting the importance of the local properties of the base flow on this kind of instability. On the other hand, the global frequency $\omega_{g,r}$ decreases with the streamwise extent of the separation bubble and then depends on global properties of the base flow.

The global stability analysis presented in section III.B is also capable of recovering the two-dimensional global oscillator behavior, including under conditions for which this mechanism is stable. The global eigenspectrum for laminar separation bubbles on a flat plate[38,42] contains a branch of eigenmodes corresponding to traveling waves. These eigenmodes represent simultaneously the Tollmien-Schlichting (TS) and the Kelvin-Helmholtz (KH) mechanisms, as their main characteristics (local velocity profile and energy growth physics) are recovered respectively in slices where the boundary layer is attached or separated. However, the accurate computation of the wave-like eigenmodes by partial-derivative-based EVPs may be difficult. Global eigenmodes in which the perturbation (more precisely, the sensitivity region[49]) is localized in a bounded spatial region far from the boundaries of the computational domain are relatively insensitive to the location of the boundaries and the boundary conditions imposed there.[28,50] On the other hand, the spatial structure of eigenmodes representing traveling waves extends over the whole domain, including the boundaries, and can be very sensitive to the choice of domain size and boundary conditions.[51] Typically, very high resolutions are demanded by these eigenmodes in order to resolve the numerical boundary layers appearing due to the *unnatural* boundary conditions.

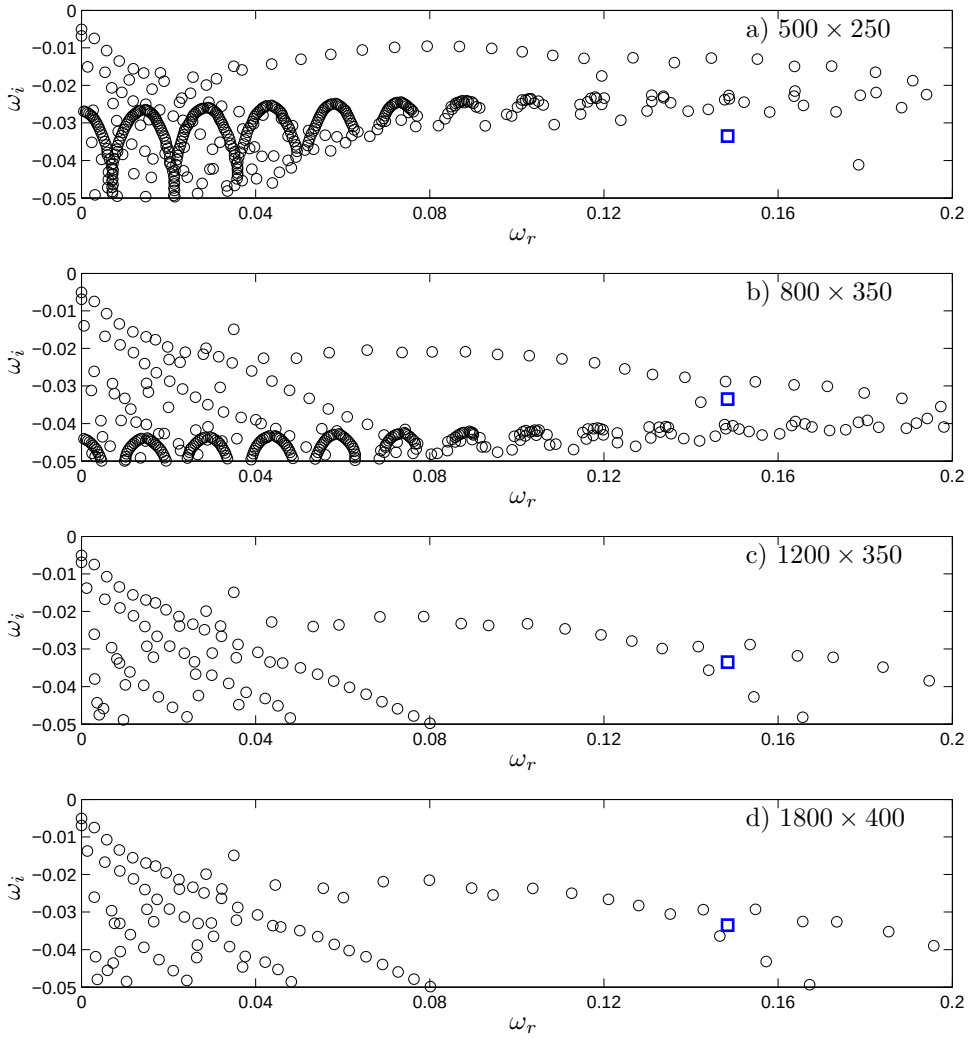

Figure 5. Global eigenspectrum of two-dimensional perturbations ($\beta = 0$) corresponding to case M8, obtained for four different spatial resolutions: (a) $N_x \times N_y = 500 \times 250$, (b) $N_x \times N_y = 800 \times 350$, (c) $N_x \times N_y = 1200 \times 350$, (d) $N_x \times N_y = 1800 \times 400$. The blue square corresponds to the global oscillator predicted by local theory, ω_g.

Figure 5 shows four eigenspectra corresponding to the same base flow (case M8), with increasing spatial resolutions. The complex frequency corresponding to the global oscillator computed using local analysis is also shown. These computations consider two-dimensional eigenmodes only ($\beta = 0$), and accordingly the spanwise momentum equation drops permitting higher resolutions at the same computational cost. Figure 5(a) corresponds to a low streamwise resolution ($N_x = 500 \times N_y = 200$), but similar to that used in similar works in the literature.[52,53] This resolution suffices for the convergence of the three-dimensional eigenmode, as will be discussed in the next section, but not for the wave-like eigenmodes: as the resolution is increased, the whole branch of TS/KH eigenmodes displaces remarkably towards more stable eigenvalues. At the highest resolution affordable in the computer used ($N_x = 1800 \times N_y = 400$, figure 5(d)), these eigenmodes seem to be close to convergence, though not fully converged yet: the splitting of the branch towards higher frequencies was pointed out[51] to be an indication that even higher resolutions are required. However, the evolution of the TS/KH branch as the resolution increases suggests that one eigenmode will converge to a value close to the global oscillator predicted by local analysis. It can be concluded that non-parallel effects are small and local analysis is a valid approach in the study of Tollmien-Schlichting and Kelvin-Helmholtz mechanisms in laminar separation bubbles, in line previous findings in the literature.[9] Consequently, the present local analysis based on the WKB assumption is believed to deliver accurate predictions of the global oscillator dynamics. Note, however, that the global oscillator predicted by local analysis does not correspond

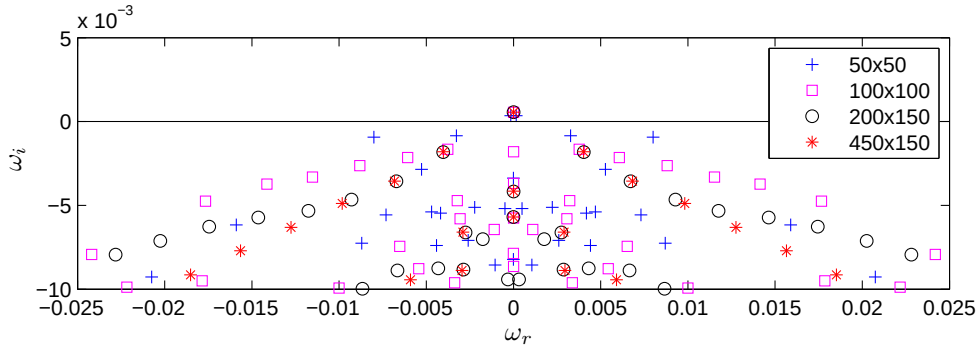

Figure 6. Global eigenspectrum of three-dimensional perturbations for $\beta = 0.22$ corresponding to case M8, obtained for four different spatial resolutions: (a) $N_x \times N_y = 50 \times 50$, (b) $N_x \times N_y = 100 \times 100$, (c) $N_x \times N_y = 200 \times 150$, (d) $N_x \times N_y = 450 \times 150$.

Table 1. Convergence history of the unstable eigenmode for $\beta = 0.22$, corresponding to case M8.

N_x	N_y	ω_i
50	50	0.000346910
100	150	0.000551547
150	150	0.000557983
200	200	0.000561056
450	150	0.000561291
400	250	0.000561358
400	300	0.000561353

to the least damped global eigenmodes within the TS/KH branch.

Figure 9(a) shows the streamwise velocity component corresponding to the stable global oscillator mode corresponding to the case M8, and compares it with the most unstable three-dimensional eigenfunction for the same base flow (figure 9(b)), discussed in the next section.

B. Steady three-dimensional global mode

Steady, two-dimensional laminar separation bubbles can become unstable to three-dimensional perturbations if the recirculation is strong enough, in terms of peak reversed flow or minimum wall shear.[23,24] A centrifugal instability appears then, which is recovered as a single discrete eigenmode in the framework of the PDE-based global instability analysis.

Figure 6 and table 1 show the convergence history of the leading eigenmodes for a representative eigenspectra. The same case M8 as in figure 5 is considered here, but for three-dimensional perturbations with $\beta = 0.22$, corresponding to the maximum temporal amplification. The convergence of the unstable eigenmode requires spatial resolutions significantly lower than the branch of TS/KH eigenmodes.

The growth rate ω_i as a function of the spanwise wavenumber β is shown for each separation bubble model in figure 7. Consistently with results in the literature, this eigenmode is unstable for a bounded range of β values, and attains the maximum amplification rate for a finite spanwise wavenumber. Identical behavior is found for the three streamwise extents of the deceleration, but the dominant wavenumber decreases as the deceleration length increases, denoting a relation between the characteristic streamwise length of the base bubble and the spanwise wavelength of the instability. Figure 8 shows the neutral curves corresponding to the three deceleration lengths, as function of spanwise wavenumber and peak reversed flow. The reversed flow, and not a Reynolds number, is consider here again to be the critical parameter for the instability, provided that the underlying physical mechanism, a centrifugal instability, is also inviscid in nature and the Reynolds numbers considered are high enough for the viscous damping to be unimportant. The critical peak recirculation, i.e. the value of the reversed flow u_{rev} for which the eigenmode becomes unstable, changes from one streamwise extent to other, but is well below $u_{\text{rev}} = 10\%$ in the cases considered. Figure 9 shows

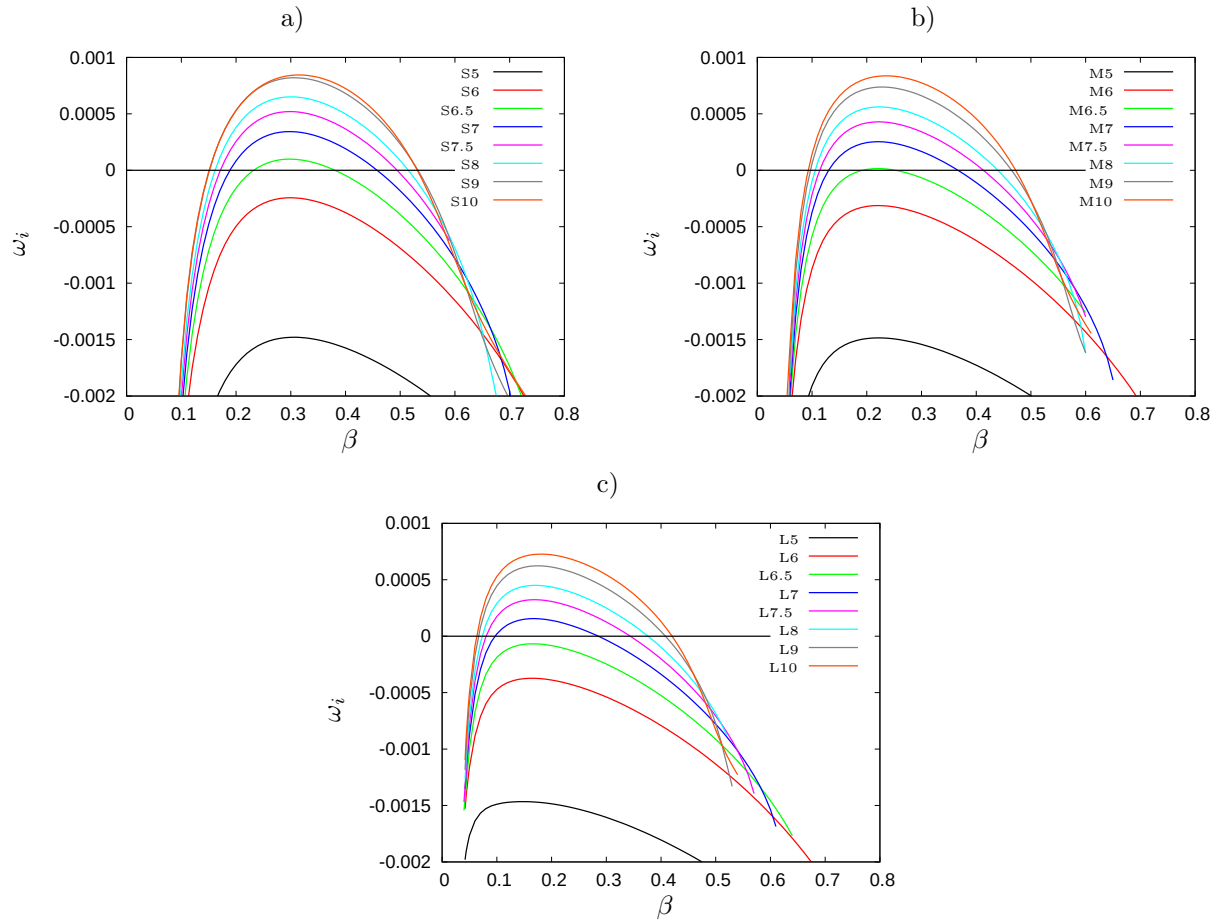

Figure 7. Temporal amplification rate ω_i against spanwise wavenumber β for the steady three-dimensional global mode. a) S cases; b) M cases; c) L cases.

the streamwise and spanwise velocity components corresponding to the three-dimensional instability for a characteristic case.

Topological reconstructions of the flow field resulting from the amplification of the centrifugal eigenmode demonstrated that this instability leads to the breakdown of the base two-dimensional bubble into independent spanwise-periodic separation regions.[28] The resulting topologies suggest that the steady centrifugal instability is responsible for the three-dimensional separation structures observed experimentally[54,55] on iced airfoils. An analogous work[29] considering a stalled NACA 0015 airfoil, a geometry for which trailing edge stall occurs, revealed the presence of a centrifugal unstable eigenmode akin to the present one; the flow topologies originated by the instability also related the three-dimensional instability of separation bubbles to the stall cells.[30,32,56]

V. Conclusions

The linear global instability of a series of model laminar separation bubbles is analyzed here, with the aim of determining the possible routes to three-dimensionalization and unsteadiness of nominally two-dimensional base states. Attention is focused on the two main global mechanisms that have been proposed in the literature, namely the behavior of the separated region as a global oscillator due to spatial regions of absolute instability of planar waves, driven by the Kelvin-Helmholtz mechanism; and the steady three-dimensionalization of the flow exerted by a steady centrifugal eigenmode. The main objective of the analyses is the determination of the primary instability, i.e. which of the two global mechanisms becomes active first, as the strength of the recirculation region increases. Both kinds of instabilities are of inviscid nature, and

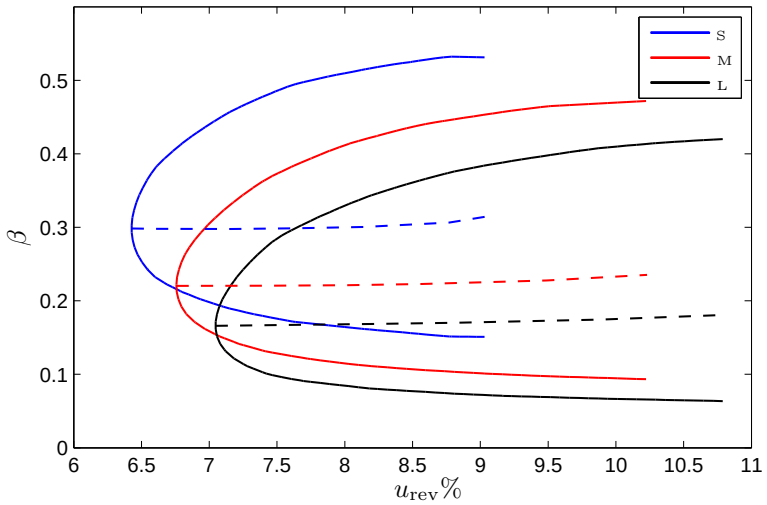

Figure 8. Neutral curves (solid lines) for the steady three-dimensional global mode, depending on the spanwise wavenumber β and the peak reversed flow $u_{\mathrm{rev}}\%$, for the the three deceleration lengths. The dashed lines correspond to the most amplified spanwise wavenumber.

the Reynolds number is expected to have a very limited effect as long as it is high enough. In line with other works in the literature, the peak reversed flow u_{rev} was used here as a measure of the bubble strength.

Two different methodologies for linear instability analyses have been employed. The first one, based on a WKBJ approximation and local instability eigenvalue problems, is concluded to be more appropriate to the study of the oscillator behavior. The second methodology, based on the solution of two-dimensional eigenvalue problems that do not impose a particular behavior to the perturbation shapes, enables the study of non wave-like perturbations like the steady three-dimensional instability. The oscillator behavior can also be studied using this methodology, but prohibitively high resolutions seem to be required for the convergence of the eigenspectra. Some works in the literature[52,53] addressing the instability of similar laminar separation bubbles, employed spatial resolutions lower than those employed here. The convergence study presented here suggests that the temporal amplification of wave-like eigenmodes (i.e. the presence of an unstable global oscillator) observed in those works might be an artifact of under-resolutions.

The present analyses show that the instability of planar disturbance waves is only of convective nature for all the model laminar separation bubble considered, a result in line with their relatively low recirculation $u_{\mathrm{rev}} < 12\%$ compared to the $u_{\mathrm{rev}} \approx 20\%$ threshold values found in the literature[9,20,21,34,36] for the onset of absolute instability. On the other hand, the three-dimensional, centrifugal mechanism becomes linearly unstable about $u_{\mathrm{rev}} \approx 7\%$. The trends observed on the global growth rates for both global instability mechanisms as the peak reversed flow or the separated region extent increase do not indicate that the oscillator mechanism would become unstable and dominate over the three-dimensionalization if longer separation bubbles were considered. It is concluded that the primary instability mechanism acting on laminar separation bubbles on a flat-plate boundary layer is a steady three-dimensionalization of the base flow, rather than a two-dimensional vortex-shedding originated by local instability of the shear-layer. Recent experimental observations in the separated boundary-layer flow after a bump[57] show the same bifurcation path. These findings are also in line with three-dimensional direct numerical simulations of flat-plate laminar separation bubbles[34,36] showing unsteadiness at $u_{\mathrm{rev}} \leq 10\%$, while two-dimensional simulations require the $u_{\mathrm{rev}} \approx 20\%$ reversed flow mentioned before.

Acknowledgments

Discussions with Prof. V. Theofilis are kindly acknowledged. D. Rodríguez acknowledges funding from the European Union Marie Curie - COFUND programme. The work of E. M. Gennaro is supported by CNPq/Brazil.

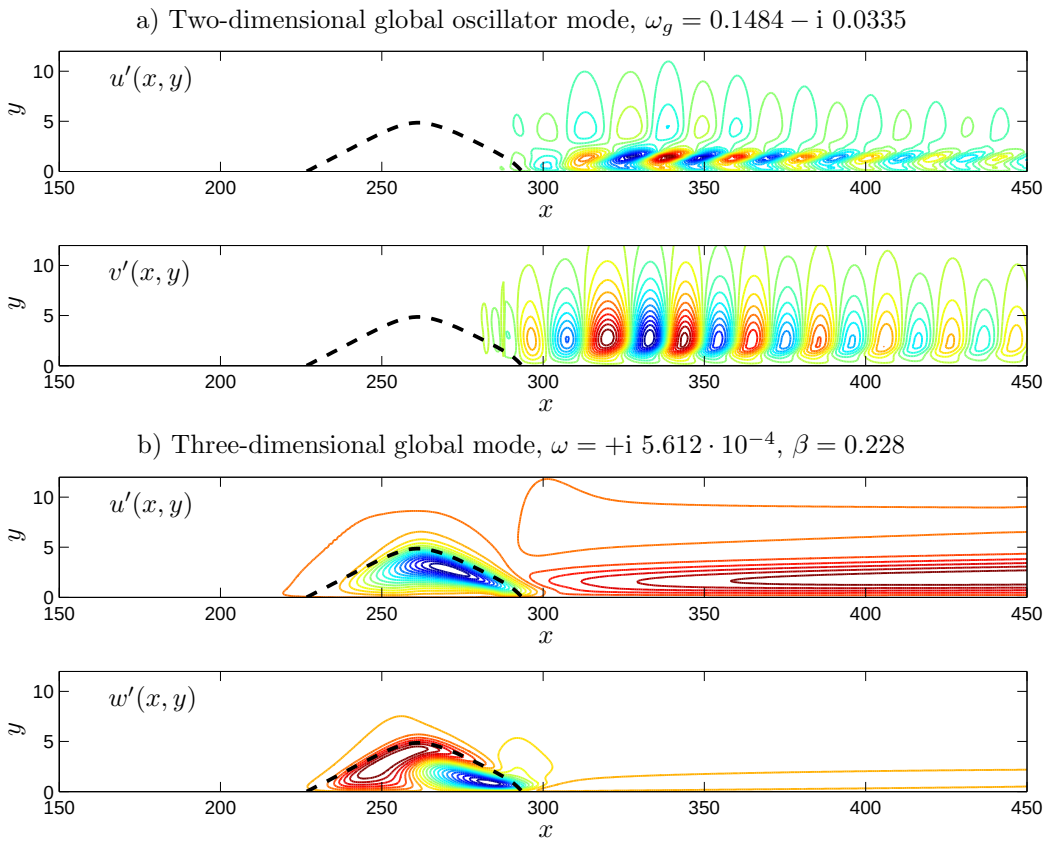

Figure 9. Perturbation velocity components corresponding to the global oscillator mode (up) and the most unstable three dimensional global instability, for the case M8. The black dashed line shows the separation streamline of the base flow.

References

[1]D. Gault, Boundary-layer and stalling characteristics of the NACA 63-009 airfoil section., NACA TN 1894.

[2]G. McCullough, D. Gault, Boundary-layer and stalling characteristics of the NACA $64_A - 006$ airfoil section., NACA TN 1923.

[3]G. McCullough, D. Gault, Examples of three representative types of airfoil-section stall at low speed, NACA TN 2502.

[4]M. Gaster, The structure and behaviour of separation bubbles, Tech. Rep. 3595, NPL Rep- & Memoranda.

[5]I. Tani, Low-speed flows involving bubble separations, Prog. Aero. Sci. 5 (1964) 70.

[6]L. Pauley, P. Moin, W. Reynolds, The structure of two-dimensional separation, J. Fluid Mech. 220 (1990) 397–411.

[7]S. Diwan, S. Chetan, O. Ramesh, On the bursting criterion for laminar separation bubbles, in: R. Govindarajan (Ed.), Sixth IUTAM Symposium on Laminar-turbulent transition, Springer, 2006, pp. 401–407.

[8]O. Marxen, D. S. Henningson, The effect of small-amplitude convective disturbances on the size and bursting of a laminar separation bubble, J. Fluid Mech. 671 (2011) 1–33.

[9]U. Rist, U. Maucher, Direct numerical simulation of 2–d and 3–d instability waves in a laminar separation bubble, in: B. Cantwell (Ed.), AGARD-CP-551 Application of Direct and Large Eddy Simulation to Transition and Turbulence, 1994, pp. 34–1 – 34–7.

[10]O. Marxen, Numerical studies of physical effects related to the controlled transition process in laminar separation bubbles, Ph.D. thesis, Stuttgart University (2004).

[11]A. Dovgal, V. Kozlov, A. Michalke, Laminar boundary layer separation: instability and associated phenomena, Prog. Aero. Sci. 3 (1994) 61–94.

[12]D. Greenblatt, I. Wygnanski, The control of flow separation by periodic excitation, Prog. Aero. Sci. 36(7) (2000) 487–545.

[13]K. Gruber, H. Bestek, H. Fasel, Interaction between a Tollmien-Schlichting wave and a laminar separation bubble, no. AIAA Paper 87-1256, 1987.

[14]O. Marxen, M. Lang, U. Rist, Discrete linear local eigenmodes in a separating laminar boundary layer, J. Fluid Mech.

[15]P. Monkewitz, P. Huerre, J. M. Chomaz, Global linear stability analysis of weakly non-parallel shear flows, J. Fluid Mech. 251 (1993) 1–20.

[16]P. Huerre, P. Monkewitz, Local and global instabilities in spatially developing flows, Ann. Rev. of Fluid Mechanics 22 (1990) 473–537.

[17]V. Theofilis, Advances in global linear instability analysis of nonparallel and three dimensional flows, Prog. Aero. Sci. 39 (2003) 249–315.

[18]V. Theofilis, Global linear stability, Ann. Rev. of Fluid Mechanics 43 (2011) 319–352.

[19]P. Huerre, P. Monkewitz, Absolute and convective instabilities in free shear layers, J. Fluid Mech. 159 (1985) 151–168.

[20]T. Allen, N. Riley, Absolute and convective instabilities in separation bubbles, Aeronautical Journal 99 (1995) 439–448.

[21]D. Hammond, L. Redekopp, Local and global instability properties of separation bubbles, Eur. J. Mech. B/Fluids 17 (1998) 145–164.

[22]U. Dallmann, G. Schewe, On topological changes of separating flow structures at transition reynolds numbers, no. Paper 87-1266 in 16th Fluid Dynamics, Plasma Dynamics and Lasers Conference, AIAA, Honolulu, HI, 1987.

[23]V. Theofilis, S. Hein, U. Dallmann, On the origins of unsteadiness and three-dimensionality in a laminar separation bubble., Phil. Trans. Roy. Soc. London (A) 358 (2000) 3229–3246.

[24]D. Barkley, M. G. M. Gomes, R. D. Henderson, Three-dimensional instability in a flow over a backward-facing step, J. Fluid Mech. 473 (2002) 167–190.

[25]F. Gallaire, M. Marquillie, U. Ehrenstein, Three-dimensional transverse instabilities in detached boundary layers, J. Fluid Mech. 571 (2007) 221–233.

[26]N. Abdessemed, S. Sherwin, V. Theofilis, Linear instability analysis of low-pressure turbine flows, J. Fluid Mech. 628 (2009) 57–83.

[27]V. Kitsios, D. Rodríguez, V. Theofilis, A. Ooi, J. Soria, Biglobal stability analysis in curvilinear coordinates of massively separated lifting bodies, J. Comp. Phys. 228 (2009) 7181–7196.

[28]D. Rodríguez, V. Theofilis, Structural changes of laminar separation bubbles induced by global linear instability, J. Fluid Mech. 655 (2010) 280–305.

[29]D. Rodríguez, V. Theofilis, On the birth of stall cells on airfoils, Theor. Comp. Fluid Dyn. 25 (2011) 105–117.

[30]D. Weihs, J. Katz, Cellular patterms in poststall flow over unswept wings, AIAA J. 21 (12) (1983) 1757–1759.

[31]S. Yon, J. Katz, Study of the unsteady flow features on a stalled wing, AIAA J. 36 (3) (1998) 305–312.

[32]G. Schewe, Reynolds-number effects in flow around more-or-less bluff bodies, J. Wind Eng. and Ind. Aerodyn. 89 (2001) 1267–1289.

[33]U. Rist, U. Maucher, Investigations of time-growing instabilities in laminar separation bubbles, Eur. J. Mech. B/Fluids 21 (2002) 495–509.

[34]H. F. Fasel, D. Postl, Interaction of separation and transition of three-dimensional development in boundary layer transition., in: R. Govindarajan (Ed.), Sixth IUTAM Symposium on Laminar-Turbulent Transition, Springer, 2004, pp. 71–88.

[35]J. H. Watmuff, Evolution of a wave packet into vortex loops in a laminar separation bubble, J. Fluid Mech. 397 (1999) 119–169.

[36]M. Alam, N. D. Sandham, Direct numerical simulation of 'short' laminar separation bubbles with turbulent reattachment, J. Fluid Mech. 410 (2000) 1–28.

[37]M. Gaster, Laminar separation bubbles, in: R. Govindarajan (Ed.), Sixth IUTAM Symposium on Laminar-Turbulent Transition, Springer, 2004, pp. 1–13.

[38]D. Rodríguez, Global stability of laminar separation bubbles, Ph.D. thesis, Universidad Politcnica de Madrid (2010).

[39]M. P. Juniper, O. Tammisola, F. Lundell, The local and global stability of confined planar wakes at intermediate reynolds number, J. Fluid Mech. 686 (2011) 218–238.

[40]T. Cebeci, J. Cousteix, Modeling and Computation of Boundary-Layer Flows - Solutions Manual and Computer Programs, Springer-Verlag, Berlin, 2005.

[41]J. Carter, Inverse solutions for laminar boundary-layer flows with separation and reattachment, Tech. Rep. NASA TR R-447 (1975).

[42]D. Rodríguez, V. Theofilis, On instability and structural sensitivity of incompressible laminar separation bubbles in a flat-plate boundary layer, AIAA Paper 2008-4148.

[43]P. Huerre, P. A. Monkewitz, Open shear flow instabilities. In Perspectives in Fluid Dynamics: a Collective Introduction to Current Research (ed. G. K. Batchelor, H. K. Moffatt & M. G. Worster), Cambridge University Press, 2000.

[44]J. M. Chomaz, P. Huerre, L. Redekopp, A frequency selection criterion in spatially-developing flows, Stud. Appl. Maths 84 (1991) 119144.

[45]A. J. Cooper, D. G. Crighton, Global modes and superdirective acoustic radiation in low-speed axisymmetrics jets, Eur. J. Mech. B/Fluids 19 (2000) 559–574.

[46]D. Rodríguez, V. Theofilis, Massively parallel numerical solution of the biglobal linear instability eigenvalue problem using dense linear algebra, AIAA J. 47 (10) (2009) 2449–2459.

[47]E. M. Gennaro, D. Rodríguez, M. A. F. Medeiros, V. Theofilis, Sparse techniques in global flow instability with application to compressible leading-edge flow, AIAA Journal.

[48]P. R. Amestoy, I. S. Duff, J.-Y. L'Excellent, J. Koster, A fully asynchronous multifrontal solver using distributed dynamic scheduling, SIAM J. Matrix Anal. Appl. 23 (1) (2001) 15–41.

[49]P. Schmid, D. Henningson, Stability and transition in shear flows, Springer-Verlag, 2001.

[50]F. Giannetti, P. Luchini, Structural sensitivity of the first instability of the cylinder wake, J. Fluid Mech. 581 (2007) 167–197.

[51]D. Rodríguez, A. Tumin, V. Theofilis, Towards the foundation of a global modes concept, AIAA Paper 2011-2225.

[52]U. Ehrenstein, F. Gallaire, Two-dimensional global low-frequency oscillations in a separating boundary-layer flows, J. Fluid Mech. 614 (2008) 315–327.

[53]S. Cherubini, J.-C. Robinet, P. D. Palma, The effects of non-normality and nonlinearity of the navier-stokes operator on the dynamics of a large laminar separation bubble, Phys. Fluids 22 (2010) 014102.

[54]H. Gurbacki, Ice-induced unsteady flowfield effects on airfoil performance (2003).

[55]J. Jacobs, M. B. Bragg, Particle image velocimetry measurements of the separation bubble on an iced airfoil, AIAA Paper 2006-3646, 2006.

[56]H. Bippes, M. Turk, Half model testing applied to wing above and below stall, in: Recent Contributions to Fluid Mechanics, Springer-Verlag, 1982, pp. 22–30.

[57]P.-Y. Passaggia, T. Leweke, U. Ehrenstein, Transverse instability and low-frequency flapping in incompressible separated boundary layer flows: an experimental study, J. Fluid Mech. 703 (2012) 363–373.